

# Universal dynamics of a turbulent superfluid Bose gas

A.D. García-Orozco,<sup>1</sup> L. Madeira,<sup>1,\*</sup> M.A. Moreno-Armijos,<sup>1</sup> A.R. Fritsch,<sup>2</sup>  
P.E.S. Tavares,<sup>3</sup> P.C.M. Castilho,<sup>1</sup> A. Cidrim,<sup>4</sup> G. Roati,<sup>5,6</sup> and V.S. Bagnato<sup>1,7</sup>

<sup>1</sup>*Instituto de Física de São Carlos, Universidade de São Paulo, CP 369, 13560-970 São Carlos, Brazil.*

<sup>2</sup>*Joint Quantum Institute, National Institute of Standards and Technology,  
and University of Maryland, Gaithersburg, 20899 Maryland, USA*

<sup>3</sup>*Departamento de Física, Universidade Federal de Minas Gerais, CP 702, 31270-901 Belo Horizonte, Brazil*

<sup>4</sup>*Departamento de Física, Universidade Federal de São Carlos, 13565-905 São Carlos, Brazil.*

<sup>5</sup>*Istituto Nazionale di Ottica del Consiglio Nazionale delle Ricerche (INO-CNR), 50019 Sesto Fiorentino, Italy.*

<sup>6</sup>*European Laboratory for Non-Linear Spectroscopy (LENS), 50019 Sesto Fiorentino, Italy.*

<sup>7</sup>*Hagler Fellow, Hagler Institute for Advanced Study,  
Texas A&M University, College Station, Texas 77843, USA*

(Dated: July 16, 2021)

We study the emergence of universal scaling in the time-evolving momentum distribution of a harmonically trapped three-dimensional Bose-Einstein condensate, parametrically driven to a turbulent state. We demonstrate that the out-of-equilibrium dynamics post excitation is described by a single function due to nearby non-thermal fixed points. The observed behavior connects the dynamics of a quantum turbulent state to several far-from-equilibrium phenomena. We present a controllable protocol to explore universality in such systems, obtaining scaling exponents that can serve as reference for future theoretical investigations. Our experimental results thus offer a promising route to investigate the complex dynamics of the quantum turbulent regime under a novel perspective.

*Introduction.*—Understanding how closed many-body quantum systems relax and thermalize when initially prepared far from equilibrium is one of the fundamental questions in modern physics. The topic is relevant to many areas of research, from cosmology [1] to high-energy physics [2]. However, despite intensive studies, many questions are still open. Experiments based on ultracold trapped atoms allow for a precise control and direct observation of their quantum dynamics, accelerating the progress in this direction [3–8]. At the same time, this experimental approach is boosted by theoretical models that provide a framework to describe this complex phenomenology [9–11]. In particular, it has been recently proposed that out-of-equilibrium quantum systems can be categorized into classes with universal dynamical behavior, in analogy to universality arising from thermal-fixed points in theories of phase transition [12, 13]. In this dynamical counterpart, however, universality emerges due to the presence of so-called non-thermal fixed points (NTFPs) – metastable states of the perturbed quantum many-body system. At the vicinity of these points, far-from-equilibrium systems show no traces of their initial conditions and have their dynamical evolution characterized by only a few parameters [13]. These ideas have successfully described many different out-of-equilibrium phenomena in a generalized manner [2, 9, 14–18].

A paradigmatic example of far-from-equilibrium dynamics for which such universal description is predicted to hold is the quantum turbulent regime in quantum fluids [9]. Quantum turbulence arises when many quantum vortices tangle with one another [19–24] and also when non-linear density waves combine randomly [25]. A dis-

tinctive hallmark of the turbulent regime is the emergence of an energy cascade that corresponds to an atomic momentum distribution described by a power-law over a certain range of wave numbers [20, 26]. This cascade mechanism is related to a non-dissipative, self-similar energy transfer between length scales and it reflects the nonlinear dynamics of a turbulent regime [20, 22, 27]. There are intrinsic difficulties to identify and characterize quantum turbulence in trapped Bose-Einstein condensates (BECs) based on the power-law behavior alone [22, 23], hence alternatives have been proposed, such as particle and energy fluxes [28–31] and entropy related quantities [32].

In this work, we report the observation of universal dynamics of a far-from-equilibrium three-dimensional (3D), harmonically trapped <sup>87</sup>Rb BEC, which is driven to reach a turbulent regime [19, 20]. By performing a scaling analysis of the time-evolving momentum distribution  $n(k, t)$ , we identify a self-similar and universal behavior. This can be characterized by a single universal function, with time and space rescaled by characteristic exponents,  $\alpha$  and  $\beta$ . We study how these exponents change with the excitation amplitude, obtaining the relationship  $\alpha = 3\beta$  for a certain range of time and excitation amplitudes, in agreement with theoretical predictions of related homogeneous systems [16]. We also verify that three different excitation amplitudes lead to the same scaling, suggesting a universal behavior even for distinct initial conditions. In this context, the exponents we extract imply a direct particle cascade, not yet reported in other systems. Our observations in such a distinct scenario corroborate the generality of universal dynamics near NTFPs.

*Experimental setup.*—Our experiment begins with

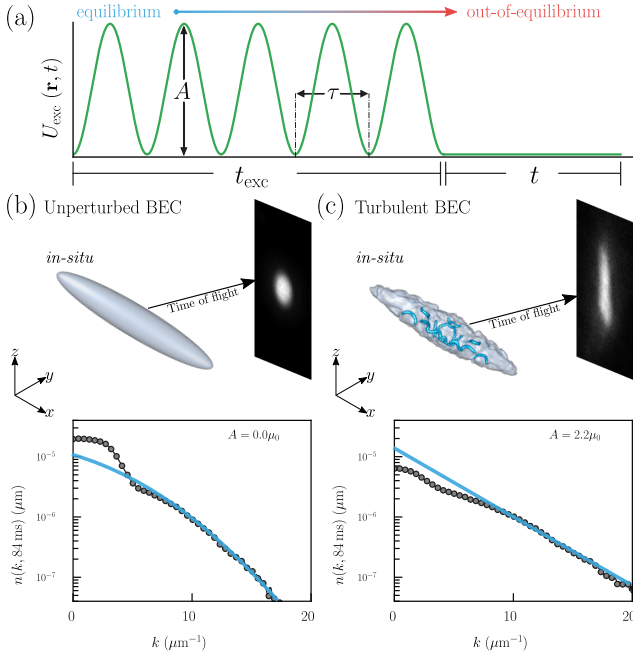


FIG. 1. (a) A controllable time-varying magnetic potential  $U_{\text{exc}}$  with amplitude  $A$  drives the BEC to an out-of-equilibrium state. The driving potential acts during an excitation time  $t_{\text{exc}}$ , corresponding to 5 driving periods  $\tau$ , and then it is turned off. The system evolves in the trap for a holding time  $t$ , during which there is no external energy input. (b)-(c) Momentum distributions for  $t = 84$  ms integrated along  $\hat{z}$ . (b) Without excitation ( $A = 0.0\mu_0$ ), the BEC is characterized by a central peak for low-momenta and a Gaussian (blue line) distribution for the thermal component. (c) When the excitation amplitude is large enough, in this case  $A = 2.2\mu_0$ , a far-from-equilibrium turbulent regime is reached, and the distribution for atoms with higher momentum shows the transition to a clear non-Gaussian distribution.

$^{87}\text{Rb}$  BECs having  $N = 2.5(3) \times 10^5$  atoms in the  $|f = 2, m_f = 2\rangle$  internal state in a Quadrupole-Ioffe configuration (QUIC) magnetic trap characterized by the frequencies  $\omega_r/2\pi = 130.7(8)$  Hz and  $\omega_x/2\pi = 21.8(2)$  Hz. The initial equilibrium BEC has a condensate fraction of 70(5)%, chemical potential  $\mu_0/k_B = 124(5)$  nK and healing length  $\xi_0 = 0.15(2)\mu\text{m}$ . To drive the BEC out of equilibrium we superimpose to the QUIC potential a controllable time-varying magnetic field gradient that creates a potential  $U_{\text{exc}}(\mathbf{r}, t) = A[1 - \cos(\Omega t)]x/R_x$ , where  $R_x = 42\mu\text{m}$  is the in-trap spatial extent of the BEC along the coordinate  $x$  of the trap, as depicted in Fig. 1(a). This is produced by an additional pair of coils in an anti-Helmholtz configuration [19]. The application of  $U_{\text{exc}}$  corresponds to an effective 3D rotation and distortion of the original trap shape [33]. We verified that our parametric drive couples the dipole mode to shape excitations, such as quadrupolar and scissor modes [34]. In the experiment, we apply a continuous oscillating drive with frequency  $\Omega/2\pi = 132.8$  Hz, during a time  $t_{\text{exc}} = 5\tau$ ,

where  $\tau = 2\pi/\Omega$ , and the amplitude  $A$  is tuned, ranging from 0 to  $2.8\mu_0$ . Using this protocol, we thus drive a BEC in initial thermal equilibrium to a far-from-equilibrium state. After the excitation is turned off, the gas is then let to evolve in the trap for variable holding times  $t$ , where the universal scaling dynamics occurs. To probe the state of the gas after a time  $t$ , we turn off the trap potential and take absorption images following the ballistic expansion of the cloud after a time of flight (ToF) of  $t_{\text{ToF}} = 30$  ms.

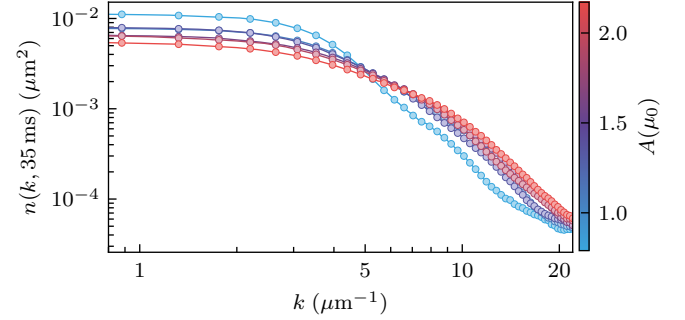


FIG. 2. Momentum distributions  $n(k, t=35$  ms) for different excitation amplitudes. The establishment of a turbulent state is supported by the power-law behavior in the momentum range  $10\mu\text{m}^{-1} \leq k \leq 17\mu\text{m}^{-1}$ .

*Out-of-equilibrium distributions.*— The momentum distribution  $\tilde{n}(k, t)$  is obtained from the two-dimensional projection of the cloud, as explained in [35]. Averaging and appropriately transforming position into momentum  $k$  as in  $r = \hbar t_{\text{ToF}}k/m$ , we obtain the *in-situ* momentum distributions  $\tilde{n}(k)$  for each instant  $t$  of the evolution time after the excitation. The normalized momentum distribution is given by  $n(k, t) = \tilde{n}(k, t)/N(t)$ , where  $N(t)$  is the total number of atoms at the holding time  $t$ .

In Figs. 1(b) and (c) we show the integration of in-plane density profiles, resulting in on-axis distributions, obtained from absorption images after  $t = 84$  ms for a BEC both in equilibrium and driven by an amplitude  $A = 2.2\mu_0$ , respectively. In Fig. 1(b), the usual bimodal  $n(k)$  of a BEC in thermal equilibrium is displayed, with a high-density peak region corresponding to the occupation of a condensate fraction (the well-known Thomas-Fermi regime) and the Gaussian distribution (blue line) due to a thermal component. For a BEC driven to a turbulent state, the system exhibits a broadened momentum distribution. The central peak is shrunk as a consequence of particle removal from lower momenta. At the same time, the tails show a departure from the Gaussian shape to an exponential dependence, as depicted in Fig. 1(c). The latter is a signature of deviation from equilibrium caused by the driving potential.

In Fig. 2, we show typical momentum distributions for different excitation amplitudes  $A$  after performing an an-

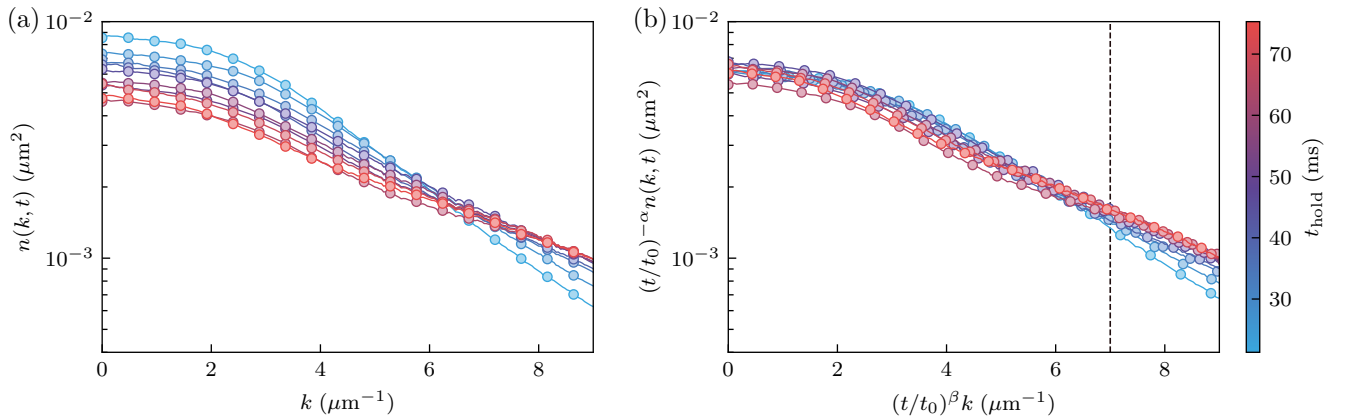


FIG. 3. (a) Momentum distribution of a turbulent state for an excitation amplitude of  $A = 1.8\mu_0$  and different holding times  $t$ . (b) After the rescaling, we see that all distributions collapse into a single curve, signaling universal dynamical behavior in the turbulent regime. The exponents characterizing this universality class are  $\alpha = -0.50(8)$  and  $\beta = -0.2(4)$ . The vertical dashed line indicates the cutoff  $k_s$  of the infrared region, where the universal scaling following Eq. (1) is observed.

gular average over the in-plane momentum shells of radius  $k$ . For fixed excitation times, as  $A$  increases, population at higher momenta grows. A power-law behavior appears in the momentum distribution,  $n(k) \propto k^{-3.1(1)}$ , over a  $k$ -range of  $10\mu\text{m}^{-1} \leq k \leq 17\mu\text{m}^{-1}$  and within the time window  $20\text{ms} \lesssim t \lesssim 70\text{ms}$  for all excitation amplitudes. This signals an energy cascade and thus the emergence of a turbulent state in the sample under consideration, as observed in other previous experiments [20]. After  $t \approx 100\text{ms}$ , the transient turbulent state decays, thus relaxing toward thermalization. For  $A \gtrsim 2.4\mu_0$ , we verified that the final state is a thermal gas, indicating that the drive has injected enough energy to fully deplete the condensate.

*Universal scaling.*—Once the system is driven out of equilibrium, we cease the parametric excitation and let the turbulent state enter a relaxation and thermalization dynamics. The temporal evolution of the system is recorded, as shown in Fig. 3(a). As we wait longer, the distribution evolves, promoting more population from low to high momentum values. We now analyze these distributions under the concept of universal dynamics exhibited by far-from-equilibrium quantum systems close to NTFPs [4, 6, 11, 13, 18]. It has been proposed [16] that far-from-equilibrium closed systems that belong to a certain universality class should exhibit their universal character through the distribution  $n(k, t)$ , which scales in time and momentum following the form

$$n(k, t) = \left(\frac{t}{t_0}\right)^\alpha F\left[\left(\frac{t}{t_0}\right)^\beta k\right], \quad (1)$$

with  $t_0$  being an arbitrary reference time within the period in which  $n(k, t)$  shows scaling properties. The  $\alpha$  and  $\beta$  exponents must be universal and independent of the initial conditions of the system. This being true, it

shows that, over a certain momentum range, the distribution  $n(k, t)$  of the decaying turbulent system depends on space and time only through a single universal function  $F(k)$ .

The rescaling of the different distributions is provided in Fig. 3(b) for the infrared region ( $k \leq k_s = 7\mu\text{m}^{-1}$ ), showing that all data for different times fall onto a single curve, with scaling exponents  $\alpha = -0.50(8)$  and  $\beta = -0.2(4)$  (see [35] for the detailed procedure on determining  $\alpha$  and  $\beta$ ). This self-similar evolution for the infrared momentum range is related to the transport of particles in our closed system during the selected time window. Self-similarity in this case requires that the particle number  $\bar{N}$  over that range of scaling is conserved. Figure 4(a) shows that this is true for all times, when the average number of particles is evaluated in the scaling region  $k \leq k_s$ . Additionally, as a consequence of the particle number being a conserved quantity in the dynamics, the average kinetic energy should increase over this same range, following  $\bar{M}_2 \propto (t/t_0)^{-2\beta}$  (see [35] and [6]). We indeed observe this buildup of the energy in the scaling region, as can be verified in Fig. 4(b).

Different excitation amplitudes,  $A = 1.8\mu_0$ ,  $2.0\mu_0$ , and  $2.2\mu_0$ , and therefore distinct initial states, lead to the same type of distribution with equivalent exponents. They thus belong to the same class of universal dynamics. For a thermally quenched 3D, isotropic and homogeneous Bose gas, numerical and analytical calculations for the infrared region have predicted the relation  $\alpha = \beta d$  (where  $d$  is the dimension of the system) [16]. Remarkably, our anisotropic, harmonically trapped system follows the same correspondence for the scaling exponents over a range of amplitudes.

Our exponents, however, do not follow the absolute values predicted in the numerical simulations of [16],

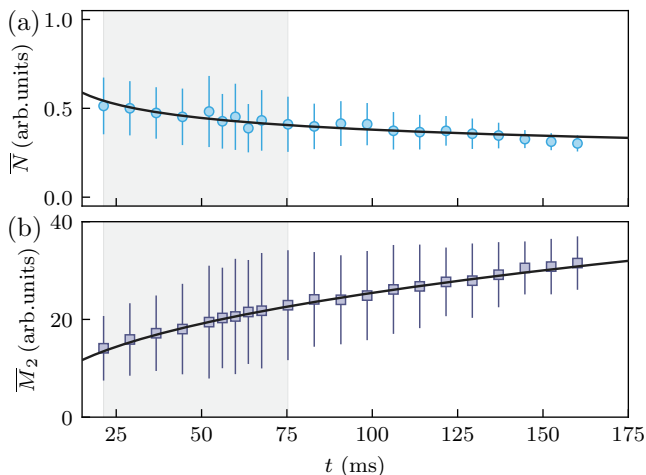


FIG. 4. Global quantities for the excitation amplitude  $A = 1.8\mu_0$ . (a) Total number of particles  $\bar{N}$  over the universality range ( $k_s \leq 7\mu\text{m}^{-1}$ ) as a function of  $t$ . The shaded region corresponds to the time window in which universal behavior is observed. (b) The mean kinetic energy  $\bar{M}_2$  increases with time over the same universal range. The curves follow the theoretical predictions, namely  $\bar{N} \propto t^{\alpha-3\beta}$  and  $\bar{M}_2 \propto t^{-2\beta}$ .

namely:  $\alpha = 1.66(12)$  and  $\beta = 0.55(3)$ . This disagreement is expected for several reasons. First of all, despite being 3D, we have a finite system in an anisotropic trap, imposing inhomogeneity over large spatial scales. Second, we provide a different route from quenching protocols to reach a far-from-equilibrium state in spinless trapped BECs. Some assumptions in [16] such as equally populating momentum states in the initial state preparation certainly does not hold in our case, and may lead the dynamics to different NTFPs. Lastly, we obtain universal scaling exponents with negative signs. This reveals a *direct* particle cascade, which has been observed in perturbative estimates [36] of turbulence thermalization. However, this is opposed to [16] and recent experiments [6, 7] of after-quench dynamics with ultracold gases. The condensation process observed in thermally quenched Bose gases, forming a quasi-condensate at intermediate times via particle-conserving transport to lower momenta, is absent here.

Surprisingly, the relation between the scaling exponents  $\alpha$  and  $\beta$  still retains the information about the system before the projection from the absorption imaging. Ideally, it would be interesting to implement experimental techniques that allow us to obtain the three-dimensional momentum distribution directly, and not only its in-plane projection as employed in this work. The correspondence  $\alpha = 3\beta$  and the influence of the projection on the values of the scaling exponents remains to be investigated in future works. Prospective studies might also focus on connecting the analysis provided here with the concept of the inverse Kibble-Zurek mechanism [37].

**Conclusion.**—We observed universal behavior in an atomic superfluid driven far from equilibrium towards a turbulent state. Our work helps us to better understand a nonequilibrium-state evolution while in the vicinity of NTFPs, closely resembling recent results obtained in other out-of-equilibrium systems [4–7]. Our presented analysis, however, shows the validity of this far-from-equilibrium theory beyond the limits explored up to this point in these other experiments. More than that, our results allow merging the quantum turbulence regime in trapped atomic gases into a class of systems that present dynamical universality by scaling. The obtained exponents can serve as reference for future theoretical studies and our cold-atom platform might be used to simulate different physical systems belonging to the same universality class.

**Acknowledgments.**—We thank A. Piñeiro Orioli, R. P. Smith, M. Caracanhas, and T. Gasenzer for fruitful discussions and G.D. Telles for support with the experimental setup. This work was supported by the São Paulo Research Foundation (FAPESP) under the grants 2013/07276-1, 2014/50857-8, 2017/09390-7, and 2018/09191-7, and by the National Council for Scientific and Technological Development (CNPq) under the grants 465360/2014-9 and 142436/2018-6.

---

\* Corresponding author: [madeira@ifsc.usp.br](mailto:madeira@ifsc.usp.br)

- [1] L. Kofman, A. Linde, and A. A. Starobinsky, *Phys. Rev. Lett.* **73**, 3195 (1994).
- [2] J. Berges, A. Rothkopf, and J. Schmidt, *Phys. Rev. Lett.* **101**, 041603 (2008).
- [3] E. Nicklas, M. Karl, M. Höfer, A. Johnson, W. Muesel, H. Strobel, J. Tomkovič, T. Gasenzer, and M. K. Oberthaler, *Phys. Rev. Lett.* **115**, 245301 (2015).
- [4] M. Prüfer, P. Kunkel, H. Strobel, S. Lannig, D. Linne-mann, C.-M. Schmied, J. Berges, T. Gasenzer, and M. K. Oberthaler, *Nature* **563**, 217 (2018).
- [5] C. Eigen, J. A. P. Glidden, R. Lopes, E. A. Cornell, R. P. Smith, and Z. Hadzibabic, *Nature* **563**, 221 (2018).
- [6] S. Erne, R. Bücke, T. Gasenzer, J. Berges, and J. Schmiedmayer, *Nature* **563**, 225 (2018).
- [7] J. A. P. Glidden, C. Eigen, L. H. Dogra, T. A. Hilker, R. P. Smith, and Z. Hadzibabic, *Nature Physics* **17**, 457 (2021).
- [8] L. Madeira and V. S. Bagnato, *Brazilian J. Phys.* **51**, 170 (2021).
- [9] C. Scheppach, J. Berges, and T. Gasenzer, *Phys. Rev. A* **81**, 033611 (2010).
- [10] M. Karl, B. Nowak, and T. Gasenzer, *Sci. Rep.* **3**, 2394 (2013).
- [11] J. Berges, K. Boguslavski, S. Schlichting, and R. Venugopalan, *Phys. Rev. Lett.* **114**, 061601 (2015).
- [12] B. Nowak, S. Erne, M. Karl, J. Schole, D. Sexty, and T. Gasenzer, *arXiv preprint* (2013), [arXiv:1302.1448](https://arxiv.org/abs/1302.1448).
- [13] M. Schmidt, S. Erne, B. Nowak, D. Sexty, and T. Gasenzer, *New J. Phys.* **14**, 075005 (2012).
- [14] B. Nowak, J. Schole, D. Sexty, and T. Gasenzer, *Phys.*



- [Rev. A \*\*85\*\*, 043627 \(2012\).](#)
- [15] B. Nowak, J. Schole, and T. Gasenzer, [New J. Phys. \*\*16\*\*, 093052 \(2014\).](#)
  - [16] A. Piñeiro Orioli, K. Boguslavski, and J. Berges, [Phys. Rev. D \*\*92\*\*, 025041 \(2015\).](#)
  - [17] C.-M. Schmied, A. N. Mikheev, and T. Gasenzer, [Int. J. Mod. Phys. A \*\*34\*\*, 1941006 \(2019\).](#)
  - [18] I. Chantesana, A. P. Orioli, and T. Gasenzer, [Phys. Rev. A \*\*99\*\*, 043620 \(2019\).](#)
  - [19] E. A. L. Henn, J. A. Seman, G. Roati, K. M. F. Magalhães, and V. S. Bagnato, [Phys. Rev. Lett. \*\*103\*\*, 045301 \(2009\).](#)
  - [20] K. J. Thompson, G. G. Bagnato, G. D. Telles, M. A. Caracanhas, F. E. A. Dos Santos, and V. S. Bagnato, [Laser Phys. Lett. \*\*11\*\*, 015501 \(2013\).](#)
  - [21] V. I. Yukalov, A. N. Novikov, and V. S. Bagnato, [J. Low Temp. Phys. \*\*180\*\*, 53 \(2015\).](#)
  - [22] M. C. Tsatsos, P. E. Tavares, A. Cidrim, A. R. Fritsch, M. A. Caracanhas, F. E. A. dos Santos, C. F. Barenghi, and V. S. Bagnato, [Phys. Rep. \*\*622\*\*, 1 \(2016\).](#)
  - [23] L. Madeira, M. Caracanhas, F. dos Santos, and V. Bagnato, [Annu. Rev. Condens. Matter Phys. \*\*11\*\*, 37 \(2020\).](#)
  - [24] L. Madeira, A. Cidrim, M. Hemmerling, M. A. Caracanhas, F. E. A. dos Santos, and V. S. Bagnato, [AVS Quantum Sci. \*\*2\*\*, 035901 \(2020\).](#)
  - [25] S. Nazarenko, *Wave turbulence*, Vol. 825 (Springer Science & Business Media, 2011).
  - [26] N. Navon, A. L. Gaunt, R. P. Smith, and Z. Hadzibabic, [Nature \*\*539\*\*, 72 \(2016\).](#)
  - [27] M. Tsubota, K. Fujimoto, and S. Yui, [J. Low Temp. Phys. \*\*188\*\*, 119 \(2017\).](#)
  - [28] A. W. Baggaley, C. F. Barenghi, and Y. A. Sergeev, [Phys. Rev. E \*\*89\*\*, 013002 \(2014\).](#)
  - [29] N. Navon, C. Eigen, J. Zhang, R. Lopes, A. L. Gaunt, K. Fujimoto, M. Tsubota, R. P. Smith, and Z. Hadzibabic, [Science \*\*366\*\*, 382 \(2019\).](#)
  - [30] A. Daniel García-Orozco, L. Madeira, L. Galantucci, C. F. Barenghi, and V. S. Bagnato, [EPL \(Europhysics Lett. \*\*130\*\*, 46001 \(2020\).](#)
  - [31] Á. V. M. Marino, L. Madeira, A. Cidrim, F. E. A. dos Santos, and V. S. Bagnato, [Eur. Phys. J. Spec. Top. \*\*230\*\*, 809 \(2021\).](#)
  - [32] L. Madeira, A. D. García-Orozco, F. E. A. dos Santos, and V. S. Bagnato, [Entropy \*\*22\*\*, 956 \(2020\).](#)
  - [33] E. A. L. Henn, J. A. Seman, E. R. F. Ramos, M. Caracanhas, P. Castilho, E. P. Olímpio, G. Roati, D. V. Magalhães, K. M. F. Magalhães, and V. S. Bagnato, [Phys. Rev. A \*\*79\*\*, 043618 \(2009\).](#)
  - [34] K. W. Madison, F. Chevy, V. Bretin, and J. Dalibard, [Phys. Rev. Lett. \*\*86\*\*, 4443 \(2001\).](#)
  - [35] See Supplemental Material at [URL will be inserted by publisher] for details on: the measurement of the integrated momentum distribution; the extraction of scaling exponents.
  - [36] R. Micha and I. I. Tkachev, [Phys. Rev. D \*\*70\*\*, 043538 \(2004\).](#)
  - [37] V. Yukalov, A. Novikov, and V. Bagnato, [Phys. Lett. A \*\*379\*\*, 1366 \(2015\).](#)
  - [38] M. Caracanhas, A. L. Fetter, G. Baym, S. R. Muniz, and V. S. Bagnato, [J. Low Temp. Phys. \*\*170\*\*, 133 \(2013\).](#)

# Supplemental Material: Universal dynamics of a turbulent superfluid Bose gas

## MEASUREMENT OF THE MOMENTUM DISTRIBUTION

The momentum distribution  $n(k)$  of the gas is measured after a finite time of flight (ToF) of ballistic expansion,  $t_{\text{ToF}} = 30$  ms. The atoms are detected using standard absorption imaging, which gives access to the density distribution in ToF,  $n(r)$ . During the expansion the momentum of the particles is approximately conserved, thus the density distribution after expansion converges to the in situ momentum distribution of the cloud. Therefore,  $n(k)$  is obtained from  $n(r)$  by defining  $k \equiv mr/(\hbar t_{\text{ToF}})$ . The ToF technique requires a kinetic-energy-dominated state to accurately provide the in situ momentum distribution of the cloud, such is the case of a turbulent state [38]. In practical terms, this can be achieved for  $t_{\text{ToF}}$  sufficiently larger than  $mR/(\hbar k)$ , where  $R$  is the in situ cloud size. The validity of this method has been extensively discussed in the literature, and this technique has been used successfully to obtain the momentum distribution of turbulent trapped BECs in previous works [20, 26].

We assess the validity of this method by changing the expansion time and comparing the resulting distributions, as shown in Fig. S1 for (a) a quasi-pure BEC and (b) an out-of-equilibrium BEC. In both panels of Fig. S1, after  $t_{\text{ToF}} = 28$  ms all  $n(k)$  curves converge to the same distribution within the experimental uncertainty.

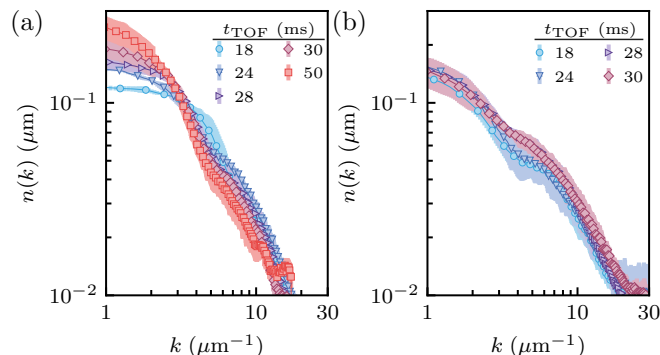


FIG. S1. Momentum distributions changing the time of flight ( $t_{\text{ToF}}$ ) for (a) a quasi-pure BEC and (b) an out-of-equilibrium BEC. The momentum distribution converges rapidly for high- $k$ . The  $n(k)$  curves overlap for  $t_{\text{ToF}} \geq 28$  ms, which is consistent with  $mR/(\hbar k)$ . The shaded regions correspond to the experimental uncertainties.

## SCALING EXPONENTS

We extracted the universal scaling exponents in Eq. (1) following closely the procedure adopted in Ref. [6], which was done in the context of a far-from-equilibrium one-dimensional Bose gas emerging from a strong cooling quench of a three-dimensional system. We minimized the function

$$\chi^2(\alpha, \beta) = \frac{1}{N_t^2} \sum_{t=t_1}^{t_{N_t}} \sum_{t_0=t_1}^{t_{N_t}} \chi_{\alpha, \beta}^2(t, t_0), \quad (\text{S1})$$

where we average both the times  $t$  and reference times  $t_0$  over all the  $N_t$  holding times  $\{t_1, \dots, t_{N_t}\}$ . The function  $\chi_{\alpha, \beta}^2(t, t_0)$  is given by

$$\chi_{\alpha, \beta}^2(t, t_0) = \int_{k_i}^{k_f} dk \frac{[(t/t_0)^\alpha n((t/t_0)^\beta k, t_0) - n(k, t)]^2}{\sigma((t/t_0)^\beta k, t_0)^2 + \sigma(k, t)^2}, \quad (\text{S2})$$

where  $\sigma(k, t)$  corresponds to the standard deviation of the mean. As explained in the main text,  $n(k, t)$  and  $\sigma(k, t)$  are normalized by the total number of atoms,  $n(k, t) = \tilde{n}(k, t)/N(t)$  and  $\sigma(k, t) = \tilde{\sigma}(k, t)/N(t)$ . The integration in Eq. (S2) is done over a  $k$ -range  $[k_i, k_f]$ . We chose  $k_i$  to be the lowest value available from the experimental data, and  $k_f$  was varied to guarantee that the results are independent of our choice. We found that the exponents are insensitive to variations of  $\delta k \approx 0.5 \mu\text{m}^{-1}$  and  $\delta t \approx 5$  ms around  $k_f = 10 \mu\text{m}^{-1}$ , within reasonable limits.

The values of  $\alpha$  and  $\beta$  are estimated through a likelihood function,

$$L_A(\alpha, \beta) = \exp \left[ -\frac{1}{2} \chi^2(\alpha, \beta) \right], \quad (\text{S3})$$

where the subscript  $A$  is a label for the different excitation amplitudes. In Fig. S2(a)-(c) depict these functions for  $A = 1.8\mu_0$ ,  $2.0\mu_0$ , and  $2.2\mu_0$ , respectively. The values of the exponents and their uncertainties are determined from a Gaussian fit of the the marginal-likelihood functions,

$$\begin{aligned} L_{\alpha, A}(\alpha) &= \int d\beta L_A(\alpha, \beta), \\ L_{\beta, A}(\beta) &= \int d\alpha L_A(\alpha, \beta), \end{aligned} \quad (\text{S4})$$

which are shown in the bottom and left panels of Figs. S2(a)-(c). Since these amplitudes produced essentially the same exponents, the values of  $\alpha$  and  $\beta$ , and their uncertainties, reported in the main text, are estimated from the combined likelihood function,

$$L(\alpha, \beta) = \prod_A L_A(\alpha, \beta), \quad (\text{S5})$$

shown in Fig. S2(d).

In the main text we showed the rescaled momentum distributions for an excitation amplitude of  $1.8\mu_0$ . In Fig. S3 we plot the rescaling of the other two amplitudes,  $2.0\mu_0$ , and  $2.2\mu_0$ .

Two global quantities can be defined,

$$\overline{N} = \int_{|k| \leq \left(\frac{t}{t_0}\right)^{-\beta} k_s} d^d k \, n(k, t) \propto \left(\frac{t}{t_0}\right)^{\alpha-d\beta}, \quad (\text{S6})$$

$$\overline{M}_2 = \int_{|k| \leq \left(\frac{t}{t_0}\right)^{-\beta} k_s} d^d k \, k^2 \frac{n(k, t)}{\overline{N}(t)} \propto \left(\frac{t}{t_0}\right)^{-2\beta}, \quad (\text{S7})$$

where  $k_s = 7.0 \mu\text{m}^{-1}$  defines the high-momentum cutoff for the scaling region. Figure S4 shows these two quantities for  $2.0\mu_0$ , and  $2.2\mu_0$ , while the same plots for  $1.8\mu_0$  are given in the main text.

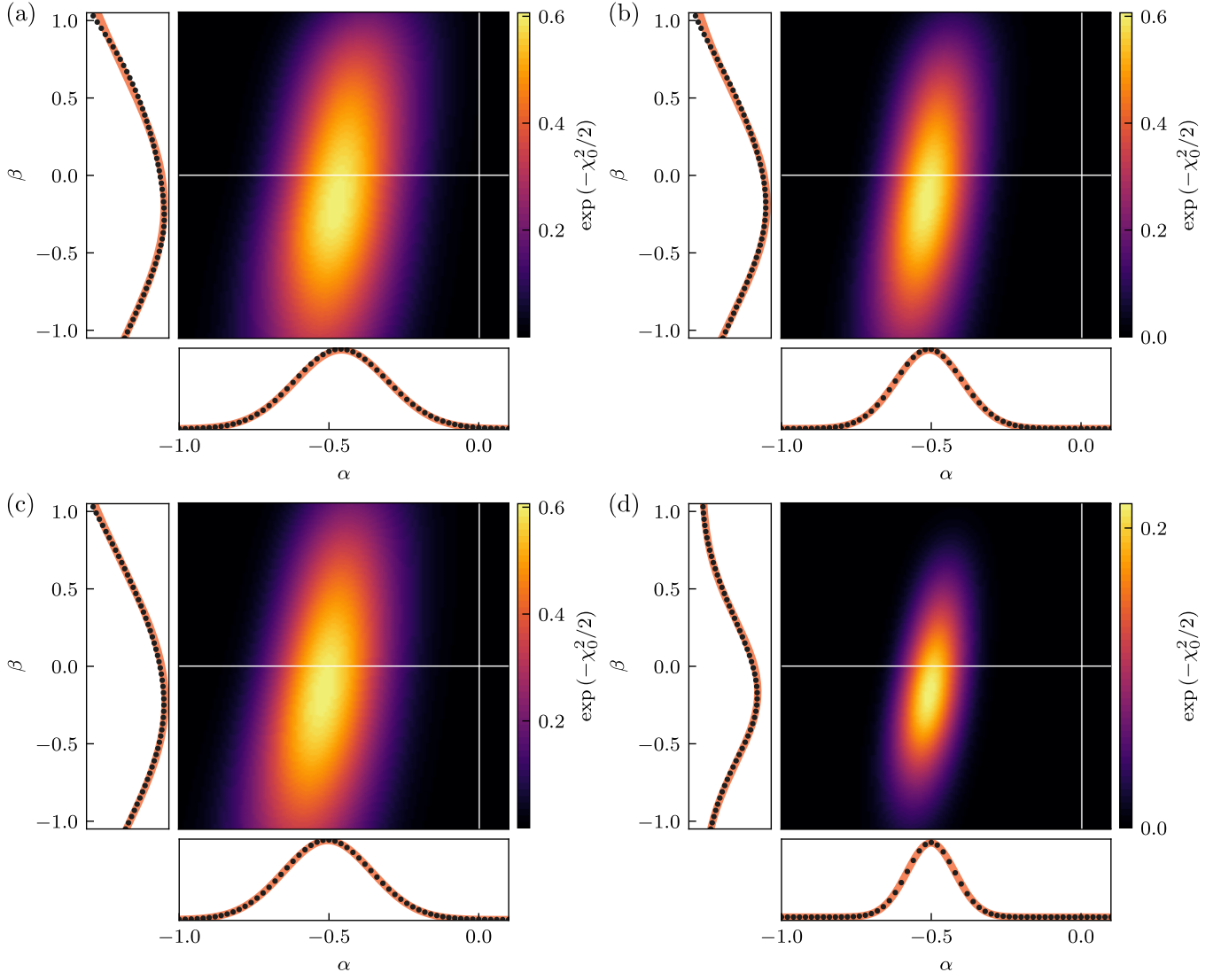


FIG. S2. Likelihood functions  $L_A(\alpha, \beta)$  for three different excitation amplitudes,  $1.8\mu_0$  (a),  $2.0\mu_0$  (b), and  $2.2\mu_0$  (c), and the product of all likelihood functions (d). For panels (a)-(c) we divide the function  $\chi^2(\alpha, \beta)$  by its minimum value, which we denote by  $\chi_0^2(\alpha, \beta)$ , so that the maximum value of  $L_A(\alpha, \beta)$  is the same for all excitation amplitudes. This choice does not affect the procedure to obtain the exponents, since the Gaussian fits to the marginal likelihood functions, shown in the left and bottom panels of each figure, are just multiplied by a constant. Notice that the combined likelihood function (d) is much more localized than the individual excitation amplitudes, as we would have expected.



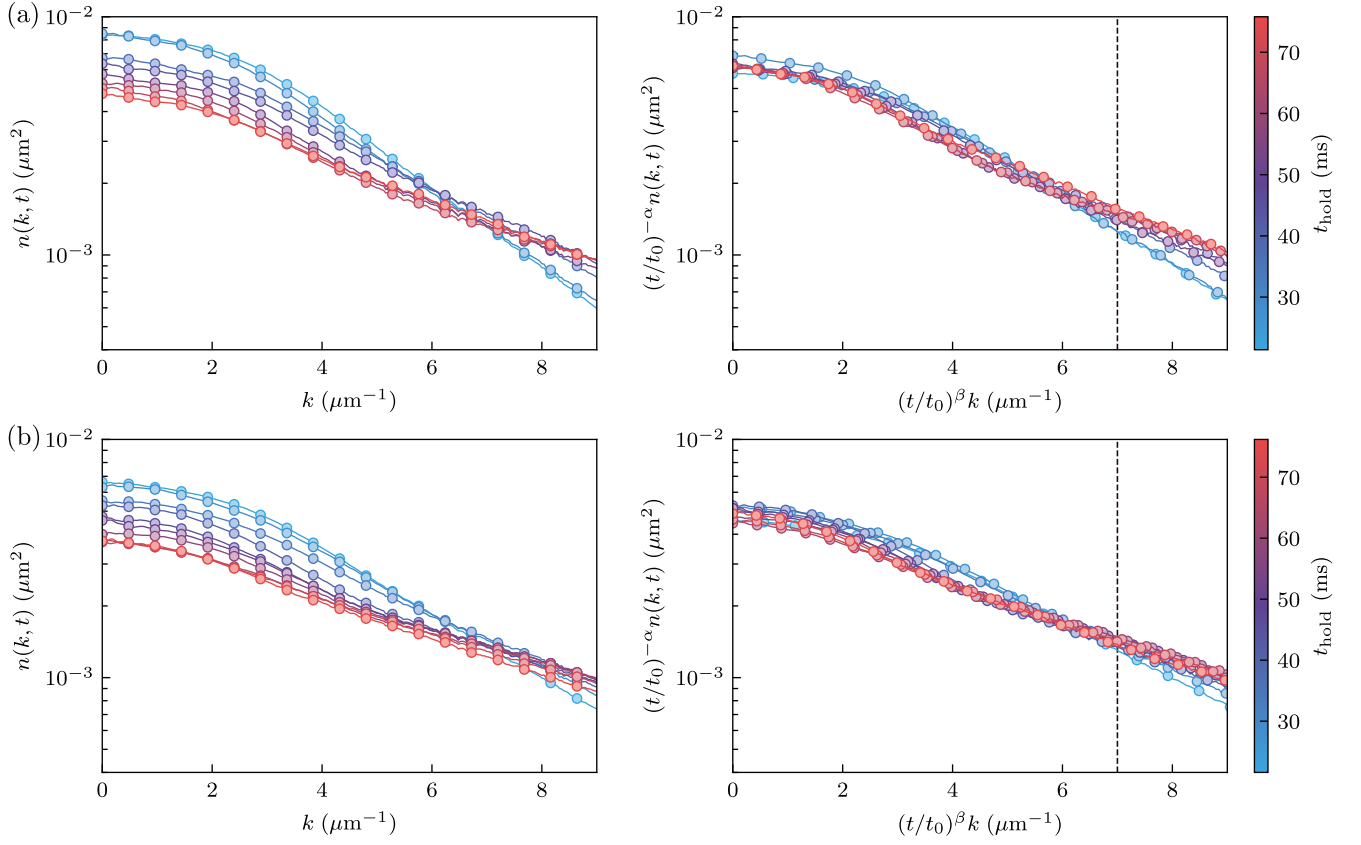


FIG. S3. Momentum distributions (left panels) and their rescaled plots (right panels) for excitation amplitudes  $A = 2.0\mu_0$  (a), and  $2.2\mu_0$  (b).

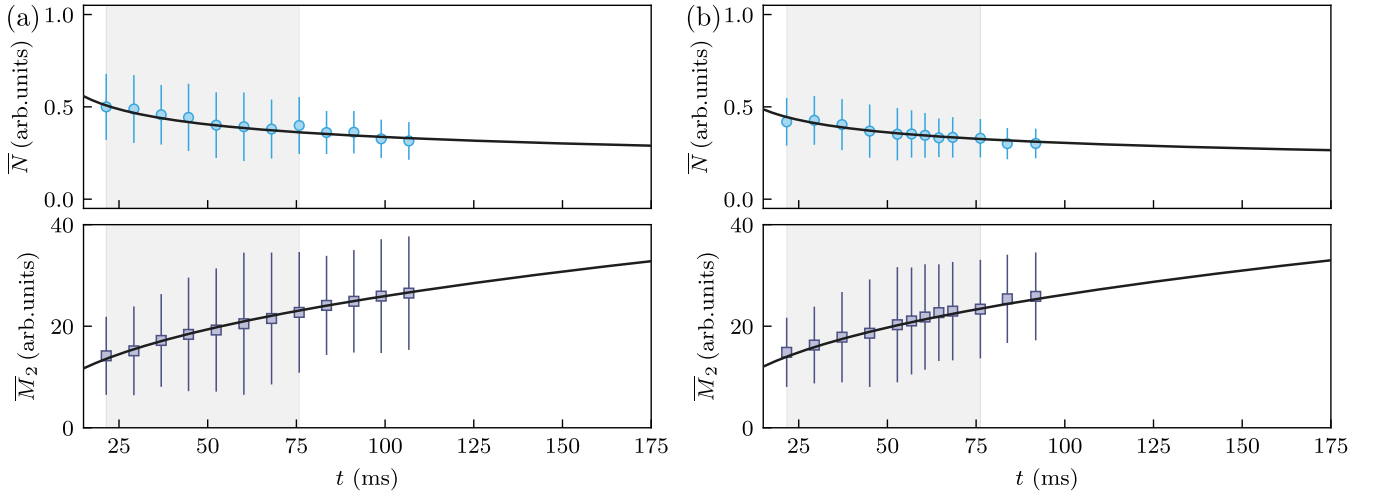


FIG. S4. Global quantities, as defined in Eqs. (S6) and (S7). The shaded region corresponds to the time interval where the universal scaling takes place. Number (top panel) and mean kinetic energy (bottom panel) for excitation amplitudes  $A = 2.0\mu_0$  (a), and  $2.2\mu_0$  (b). The curves correspond to the theoretical predictions,  $\bar{N} \propto t^{\alpha-3\beta}$  and  $\bar{M}_2 \propto t^{-2\beta}$ .